Spin polarization of electrons in a circularly polarized magnetic field

Dejia Dai *

Graduate School, China Academy of Engineering Physics, Beijing 100193, China

(Received 30 June 2023; accepted 23 October 2023; published 7 November 2023)

Recently, the spin polarization of electrons induced by magnetic dipole radiation in a circularly polarized magnetic field was investigated [O. V. Kibis, Phys. Rev. A **105**, 043106 (2022)] based on the Weisskopf-Wigner approximation. We reconsider the same subject with a more reasonable treatment of the initial magnetic field. It is found that if the electron is initially in a spin-unpolarized state, its polarization vector $\langle \boldsymbol{\sigma} \rangle$ precesses around the z axis and eventually reaches a radiation equilibrium. The corresponding stable precession frequency is the same as the external magnetic field frequency ω_0. In particular, when ω_0 is much larger than the magnetic field intensity B_0, $\langle \sigma_z \rangle$ will be close to a fixed value of about $2/3$ with time. In addition, we also analyze the influence of the parameters ω_0 and B_0 on the final polarizability. The results show that there exists a parametric region where electrons can be almost fully polarized and the required time can be reduced to the order of seconds.

DOI: 10.1103/PhysRevA.108.053109

I. INTRODUCTION

Spin-polarized electron beams are widely applied in modern scientific research. By utilizing the interaction between the spin of electrons and other particles or substances, they can serve as a powerful experimental tool in fields such as particle and nuclear physics [1–7], materials science [8–12], and atomic and molecular physics [13,14]. Consequently, it is very important to generate high-performance polarized electron beams. Since the 1970s, numerous types of polarized electron sources have been developed [15–21]. Among them, the GaAs polarized electron source [15,22] has gained widespread popularity due to its high polarizability [23], high beam intensity [24], and various other advantages [22,25]. In recent years, with the rapid development of laser technology [26], ultraintense lasers (with intensities exceeding 10^{22} W/cm^2) have been achieved in laboratory settings [27,28]. Schemes utilizing ultraintense laser pulses to generate highly polarized electron beams on the femtosecond scale have been proposed [29–31]. Such methods have significant application prospects but still require experimental verification.

Generally, when a free electron is subjected to strong electromagnetic fields, its trajectory, spin, and radiation interact with each other [32], resulting in spin polarization. Meanwhile, it is well known that the radiation dynamics of charged particles are mainly governed by three mechanisms: electric dipole radiation, electric quadrupole radiation, and magnetic dipole radiation. Among them, the former two are dependent on the spatial motion of the particles [33], while magnetic dipole radiation can exist independently. For example, when an initially stationary electron is placed in a circularly polarized magnetic field, its radiation dynamics are solely governed by magnetic dipole radiation. Recently, a study [34] calculated the spin polarizability of the electron in this case with a fully quantum method, and the results indicate that the angular momentum of the circularly polarized magnetic field can effectively transfer to the electron, leading to spin polarization. However, some conclusions of that work are not applicable to the case where the initial radiation field is a classical magnetic field. This is because the initial state of the radiation field in Ref. [34] is not a coherent state [35]. Furthermore, a similar toy model that neglects electron motion and only considers the interaction between spin and a strong field can be found in Ref. [36]. It provides some insight into the study of back-reaction effects in strong-field quantum electrodynamics.

The goal of this paper is to provide a derivation of spin polarization of electrons in a circularly polarized magnetic field. Specifically, we will not quantize the magnetic field but instead will treat it directly in its classical form. Also, we still use the Weisskopf-Wigner approximation [37,38] and derive the reduced density matrix of electrons. Through numerical simulation, we obtain some different conclusions and findings from those in Ref. [34]. These results are helpful in understanding the dynamics of electrons in a circularly polarized magnetic field.

The paper is organized as follows. In Sec. II, we describe the derivation of the spin polarizability in detail. Our numerical results are presented in Sec. III. We summarize and discuss our results in Sec. IV. Unless stated otherwise, atomic units (a.u.) with $\hbar = e = 1$ and $c \approx 137.036$ are employed throughout this paper. Here, e represents the elementary charge, and c is the speed of light.

II. METHOD

A. Dynamical equations of the system and their solutions

Let us consider a space-independent circularly polarized magnetic field, written as

$$\boldsymbol{B}_c(t) = B_0\left(e^{-i\omega_0 t}\boldsymbol{\epsilon}_0 + e^{i\omega_0 t}\boldsymbol{\epsilon}_0^*\right), \tag{1}$$

*daidejia19@gscaep.ac.cn

where B_0 and ω_0 represent the amplitude and angular frequency, $\boldsymbol{\epsilon}_0 = \frac{1}{\sqrt{2}}(\boldsymbol{e}_x + i\boldsymbol{e}_y)$ is the polarization vector, and $\boldsymbol{e}_x$ and $\boldsymbol{e}_y$ are unit vectors for the x and y axes. Such a magnetic field configuration may be achieved by a node of an electromagnetic standing wave. For example, if there is an electromagnetic standing wave, its electric field and magnetic field configurations are

$$\boldsymbol{E}_c = E_c \begin{pmatrix} \cos(k_0 z)\cos(\omega_0 t) \\ \cos(k_0 z)\sin(\omega_0 t) \\ 0 \end{pmatrix} \tag{2}$$

and

$$\boldsymbol{B}_c = B_c \begin{pmatrix} -\sin(k_0 z)\sin(\omega_0 t) \\ -\sin(k_0 z)\cos(\omega_0 t) \\ 0 \end{pmatrix}, \tag{3}$$

respectively. Here, $E_c = cB_c$ and $\omega_0 = ck_0$. When $\cos(k_0 z) = 0$, the magnetic field equation (1) can be obtained. At the same time, if the electron's initial position satisfies the condition $\cos(k_0 z) = 0$ and the initial momentum is zero, the Lorentz force will remain zero. In this case, the spatial motion of the electron can be neglected. Moreover, if the Stern-Gerlach effect is also considered, the electron will experience an additional force in the magnetic field, which can be written as

$$\boldsymbol{F}_s = -\nabla(\boldsymbol{\mu} \cdot \boldsymbol{B}_c), \tag{4}$$

where $\boldsymbol{\mu}$ represents the electron's spin magnetic moment. Clearly, combining Eq. (3) with the initial conditions just mentioned, $\boldsymbol{F}_s$ will also remain 0. Therefore the spatial motion of electrons can still be ignored.

Note that our above analysis of electrons not moving at the node where $\cos(k_0 z) = 0$ is based on classical mechanics, and whether such a node solution is stable in quantum mechanics needs to be further determined. A corresponding detailed analysis is beyond the scope of this paper. Nevertheless, the dynamics of charged scalar particles and electrons at the magnetic node where $\sin(k_0 z) = 0$ have been discussed [39,40], and the results show that the solutions of both at the magnetic node are inherently unstable.

Now let us return to the topic. If an electron with a velocity of zero is placed in the magnetic field as described in Eq. (1), the Hamiltonian of the whole system can be represented as follows:

$$H = \tfrac{1}{2}\boldsymbol{\sigma} \cdot [\boldsymbol{B}_c(t) + \boldsymbol{B}_Q(t)]. \tag{5}$$

Here, $\boldsymbol{\sigma}$ is the Pauli operator. $\boldsymbol{B}_Q(t)$ is the quantized operator for the magnetic field, and it is denoted as

$$\boldsymbol{B}_Q(t) = \sum_{\boldsymbol{k},s} B_{\boldsymbol{k},s}(e^{-i\omega t}\boldsymbol{\epsilon}_{\boldsymbol{k},s} a_{\boldsymbol{k},s} + \text{H.c}). \tag{6}$$

In Eq. (6), the Coulomb gauge is adopted; hence $\boldsymbol{k} \cdot \boldsymbol{\epsilon}_{\boldsymbol{k},s} = 0$ and $s = 1$ or 2. $B_{\boldsymbol{k},1(2)} = \pm i\sqrt{\frac{2\pi\omega_k}{Vc^2}}$, and V is the normalized volume of the field. For convenience, we can set $V = 1$. $\boldsymbol{\epsilon}_{\boldsymbol{k},s}$ is the polarization vector of the quantized field. $\omega = c|\boldsymbol{k}|$ is the angular frequency of the photon. $a_{\boldsymbol{k},s}$ represents the annihilation operator, satisfying the commutation relation $[a_{\boldsymbol{k},s}, a^\dagger_{\boldsymbol{k}',s}] = \delta_{\boldsymbol{k}\boldsymbol{k}'}\delta_{ss'}$. Here, δ is the Kronecker symbol.

The wave function $|\psi(t)\rangle$ of the system satisfies the equation

$$i\frac{\mathrm{d}|\psi(t)\rangle}{\mathrm{d}t} = \frac{1}{2}\boldsymbol{\sigma} \cdot [\boldsymbol{B}_c(t) + \boldsymbol{B}_Q(t)]|\psi(t)\rangle. \tag{7}$$

Now, we introduce the following two time-dependent wave functions [34]:

$$|g\rangle = \left[\sqrt{\frac{\Omega+\omega_0}{2\Omega}}|\uparrow\rangle - \sqrt{\frac{\Omega-\omega_0}{2\Omega}}e^{i\omega_0 t}|\downarrow\rangle\right]e^{-iE_g t},$$
$$|e\rangle = \left[\sqrt{\frac{\Omega+\omega_0}{2\Omega}}|\downarrow\rangle + \sqrt{\frac{\Omega-\omega_0}{2\Omega}}e^{-i\omega_0 t}|\uparrow\rangle\right]e^{-iE_e t}, \tag{8}$$

where $\Omega = \sqrt{2B_0^2 + \omega_0^2}$, $E_g = (\omega_0 - \Omega)/2$, $E_e = (\Omega - \omega_0)/2$, and $|\uparrow\rangle$ and $|\downarrow\rangle$ are two eigenstates of spin projected along the z axis. $|g\rangle$ and $|e\rangle$ are orthogonal to each other and normalized. Obviously, they constitute a complete basis set of the spin two-dimensional space. To solve Eq. (7), we can expand $|\psi(t)\rangle$ as follows:

$$|\psi(t)\rangle = c_e(t)|e,0\rangle + c_g(t)|g,0\rangle + \sum_{\boldsymbol{k},s}[c_{e\boldsymbol{k}s}(t)|e,1_{\boldsymbol{k},s}\rangle + c_{g\boldsymbol{k}s}(t)|g,1_{\boldsymbol{k},s}\rangle], \tag{9}$$

where $|e,0\rangle = |e\rangle \otimes |0\rangle$, $|0\rangle$ represents the vacuum state of the radiation field, and $|1_{\boldsymbol{k},s}\rangle$ denotes the occupation number of the scattered photon state on mode $\boldsymbol{k}s$ as 1. It should be noted that in Eq. (9) we omit the states in which the number of scattered photons is greater than or equal to 2, which correspond to higher-order processes. Substituting Eq. (9) into Eq. (7), we obtain

$$\begin{aligned} i\frac{\mathrm{d}}{\mathrm{d}t}c_e(t) &= \sum_{\boldsymbol{k},s} u_1(t)c_{g\boldsymbol{k}s}(t) + \sum_{\boldsymbol{k},s} w_1(t)c_{e\boldsymbol{k}s}(t), \\ i\frac{\mathrm{d}}{\mathrm{d}t}c_g(t) &= \sum_{\boldsymbol{k},s} u_2(t)c_{g\boldsymbol{k}s}(t) + \sum_{\boldsymbol{k},s} w_2(t)c_{e\boldsymbol{k}s}(t), \\ i\frac{\mathrm{d}}{\mathrm{d}t}c_{e\boldsymbol{k}s}(t) &= w_1^*(t)c_e(t) + w_2^*(t)c_g(t), \\ i\frac{\mathrm{d}}{\mathrm{d}t}c_{g\boldsymbol{k}s}(t) &= u_1^*(t)c_e(t) + u_2^*(t)c_g(t). \end{aligned} \tag{10}$$

Here,

$$\begin{aligned} u_1(t) &= \tfrac{1}{2}B_{\boldsymbol{k},s}e^{-i\omega t}\langle e|\boldsymbol{\sigma} \cdot \boldsymbol{\epsilon}_{\boldsymbol{k},s}|g\rangle, \\ u_2(t) &= \tfrac{1}{2}B_{\boldsymbol{k},s}e^{-i\omega t}\langle g|\boldsymbol{\sigma} \cdot \boldsymbol{\epsilon}_{\boldsymbol{k},s}|g\rangle, \\ w_1(t) &= \tfrac{1}{2}B_{\boldsymbol{k},s}e^{-i\omega t}\langle e|\boldsymbol{\sigma} \cdot \boldsymbol{\epsilon}_{\boldsymbol{k},s}|e\rangle, \\ w_2(t) &= \tfrac{1}{2}B_{\boldsymbol{k},s}e^{-i\omega t}\langle g|\boldsymbol{\sigma} \cdot \boldsymbol{\epsilon}_{\boldsymbol{k},s}|e\rangle. \end{aligned} \tag{11}$$

After a brief calculation, we have

$$\langle g|\boldsymbol{\sigma} \cdot \boldsymbol{\epsilon}_{\boldsymbol{k},s}|g\rangle = \frac{\omega_0}{\Omega}\cos\theta_s - \frac{\sqrt{2}B_0}{\Omega}\sin\theta_s\cos(\omega_0 t - \phi_s),$$
$$\langle e|\boldsymbol{\sigma} \cdot \boldsymbol{\epsilon}_{\boldsymbol{k},s}|e\rangle = -\frac{\omega_0}{\Omega}\cos\theta_s + \frac{\sqrt{2}B_0}{\Omega}\sin\theta_s\cos(\omega_0 t - \phi_s),$$

$$\langle e|\boldsymbol{\sigma}\cdot\boldsymbol{\epsilon}_{\boldsymbol{k},s}|g\rangle = e^{i\Omega t}\left[\frac{\omega_0}{\Omega}\sin\theta_s\cos(\omega_0 t-\phi_s) + \frac{\sqrt{2}B_0}{\Omega}\cos\theta_s - i\sin\theta_s\sin(\omega_0 t-\phi_s)\right]. \tag{12}$$

The variables θ_s and ϕ_s represent the polar angle and azimuthal angle of vector $\boldsymbol{\epsilon}_{\boldsymbol{k},s}$, respectively. According to (10), the solutions for $c_{e\boldsymbol{k}s}(t)$ and $c_{g\boldsymbol{k}s}(t)$ can be expressed in integral form as

$$\begin{bmatrix} c_{e\boldsymbol{k}s}(t) \\ c_{g\boldsymbol{k}s}(t)\end{bmatrix} = -i\int_0^t \begin{bmatrix} w_1^*(t_1) & w_2^*(t_1) \\ u_1^*(t_1) & u_2^*(t_1)\end{bmatrix}\begin{bmatrix} c_e(t_1) \\ c_g(t_1)\end{bmatrix}\mathrm{d}t_1. \tag{13}$$

Substituting the above equation into the first two equations of (10), we arrive at the expression

$$\frac{\mathrm{d}}{\mathrm{d}t}\begin{bmatrix} c_e(t) \\ c_g(t)\end{bmatrix} = -\frac{1}{(2\pi)^3}\int_0^t\int\sum_s \begin{bmatrix} f_{11} & f_{12} \\ f_{21} & f_{22}\end{bmatrix}\begin{bmatrix} c_e(t_1) \\ c_g(t_1)\end{bmatrix}\mathrm{d}\boldsymbol{k}\mathrm{d}t_1, \tag{14}$$

where

$$\begin{aligned} f_{11} &= w_1(t)w_1^*(t_1) + u_1(t)u_1^*(t_1), \\ f_{22} &= w_2(t)w_2^*(t_1) + u_2(t)u_2^*(t_1), \\ f_{12} &= w_1(t)w_2^*(t_1) + u_1(t)u_2^*(t_1), \\ f_{21} &= w_2(t)w_1^*(t_1) + u_2(t)u_1^*(t_1). \end{aligned} \tag{15}$$

Thus

$$\frac{\mathrm{d}}{\mathrm{d}t}\begin{bmatrix} c_e(t) \\ c_g(t)\end{bmatrix} = -\frac{1}{16\pi^2c^5}\int_0^t\int_0^\infty \omega^3 e^{-i\omega(t-t_1)} \times \begin{bmatrix} F_{11} & F_{12} \\ F_{21} & F_{22}\end{bmatrix}\begin{bmatrix} c_e(t_1) \\ c_g(t_1)\end{bmatrix}\mathrm{d}\omega\mathrm{d}t_1. \tag{16}$$

The derivation process of Eq. (16) and the expression of matrix element F_{ij} are elaborated in detail in Appendix A.

In order to study the long-term evolution of the system, the Weisskopf-Wigner approximation [37,38] is applied when solving Eq. (16). Consequently, we derive that

$$\frac{\mathrm{d}}{\mathrm{d}t}\begin{bmatrix} c_e(t) \\ c_g(t)\end{bmatrix} = -\frac{1}{8c^5}\begin{bmatrix} G_1 & e^{i\Omega t}G_2 \\ e^{-i\Omega t}G_3 & G_4\end{bmatrix}\begin{bmatrix} c_e(t) \\ c_g(t)\end{bmatrix}, \tag{17}$$

where

$$\begin{aligned} G_1 &= \frac{4B_0^2}{3\Omega^2}\omega_0^3 + \frac{8\Omega B_0^2}{3} + \frac{2B_0^4}{3\Omega}, \\ G_2 &= \frac{2\sqrt{2}B_0}{3\Omega}\left(1-\frac{\omega_0}{\Omega}\right)\omega_0^3, \\ G_3 &= \frac{16\sqrt{2}\omega_0 B_0^3}{3\Omega} + \frac{4\sqrt{2}\omega_0 B_0\Omega}{3} + \frac{2\sqrt{2}B_0}{3\Omega}\left(1+\frac{\omega_0}{\Omega}\right)\omega_0^3, \\ G_4 &= \frac{4B_0^2}{3\Omega^2}\omega_0^3. \end{aligned} \tag{18}$$

Now, solving Eq. (17) is straightforward. First, we can express $c_g(t)$ in terms of $c_e(t)$, that is,

$$c_g(t) = e^{-i\Omega t}\dot{c}_e(t)/G_2 - e^{-i\Omega t}c_e(t)G_1/G_2. \tag{19}$$

Then, substituting (19) back into (17) yields

$$\ddot{c}_e(t) - \rho_1\dot{c}_e(t) + \rho_2 c_e(t) = 0, \tag{20}$$

where

$$\begin{aligned} \rho_1 &= i\Omega + G_1 + G_4, \\ \rho_2 &= i\Omega G_1 + G_1G_4 - G_2G_3. \end{aligned} \tag{21}$$

The general solution of Eq. (20) is given by

$$c_e(t) = h_1e^{\lambda_1 t} + h_2e^{\lambda_2 t}. \tag{22}$$

Here,

$$\begin{aligned} \lambda_1 &= \frac{\rho_1 + \sqrt{\rho_1^2 - 4\rho_2}}{2}, \\ \lambda_2 &= \frac{\rho_1 - \sqrt{\rho_1^2 - 4\rho_2}}{2}. \end{aligned} \tag{23}$$

Furthermore, by considering the initial conditions, we have

$$\begin{aligned} h_1 &= \frac{(G_1-\lambda_2)c_e(0) + G_2c_g(0)}{\lambda_1-\lambda_2}, \\ h_2 &= \frac{(\lambda_1-G_1)c_e(0) - G_2c_g(0)}{\lambda_1-\lambda_2}. \end{aligned} \tag{24}$$

Finally, substituting (22) into (19), $c_g(t)$ is given by

$$c_g(t) = h_3e^{\lambda_3 t} + h_4e^{\lambda_4 t}, \tag{25}$$

and the correlation coefficients $h_{3,4}$ and $\lambda_{3,4}$ are as follows:

$$\begin{aligned} \lambda_3 &= \lambda_1 - i\Omega, \\ \lambda_4 &= \lambda_2 - i\Omega, \\ h_3 &= h_1(\lambda_1 - G_1)/G_2, \\ h_4 &= h_2(\lambda_2 - G_1)/G_2. \end{aligned} \tag{26}$$

B. Reduced density matrix of electrons

In Sec. II A, we introduce the procedure for solving Eq. (7). However, this only applies to the case where the initial state of the system is a pure state. In general, when the electron is initially in a mixed state, the initial density matrix $\rho_S(0)$ of the entire system can be written as

$$\rho_S(0) = (p_1|\varphi_+\rangle\langle\varphi_+| + p_2|\varphi_-\rangle\langle\varphi_-|)\otimes|0\rangle\langle 0|. \tag{27}$$

In the above formula,

$$p_1 = \frac{1+|\boldsymbol{P}_0|}{2}, \quad p_2 = \frac{1-|\boldsymbol{P}_0|}{2}, \tag{28}$$

where $\boldsymbol{P}_0$ is the polarization vector of the electron at $t=0$. $\varphi_\pm$ are two eigenstates of the operator $\sigma_0 = \boldsymbol{\sigma}\cdot\boldsymbol{P}_0/|\boldsymbol{P}_0|$, that is, $\sigma_0\varphi_\pm = \pm\varphi_\pm$.

Meanwhile, the time evolution of the density matrix is given by

$$\rho_S(t) = U(t)\rho_S(0)U^\dagger(t), \tag{29}$$

where $U(t)$ is the time evolution operator and it satisfies

$$i\frac{\mathrm{d}U(t)}{\mathrm{d}t} = HU(t). \tag{30}$$

Clearly, we can now transform $\rho_S(t)$ into

$$\rho_S(t) = p_1|\psi_+(t)\rangle\langle\psi_+(t)| + p_2|\psi_-(t)\rangle\langle\psi_-(t)| \tag{31}$$

by using Eq. (30). Here, both $|\psi_+(t)\rangle$ and $|\psi_-(t)\rangle$ satisfy Eq. (7), and their corresponding initial states are $|\varphi_+, 0\rangle$ and $|\varphi_-, 0\rangle$, respectively. As a result, the reduced density matrix ρ_e of electrons is given by

$$\begin{aligned}\rho_e &= \mathrm{tr}_L[\rho_S(t)] \\ &= \sum_{n=1}^{2} p_n \begin{pmatrix} |f_0|^2 + \sum_{\boldsymbol{k},s}|f_{\boldsymbol{k},s}|^2 & f_0 g_0^* + \sum_{\boldsymbol{k},s} f_{\boldsymbol{k},s} g_{\boldsymbol{k},s}^* \\ f_0^* g_0 + \sum_{\boldsymbol{k},s} f_{\boldsymbol{k},s}^* g_{\boldsymbol{k},s} & |g_0|^2 + \sum_{\boldsymbol{k},s}|g_{\boldsymbol{k},s}|^2 \end{pmatrix},\end{aligned} \tag{32}$$

where tr_L represents the trace operation on the photon state and

$$\begin{aligned} f_0 &= xe^{-iE_g t}c_g(t) + ye^{-i(E_e+\omega_0)t}c_e(t), \\ g_0 &= -ye^{-i(E_g-\omega_0)t}c_g(t) + xe^{-iE_e t}c_e(t), \\ f_{\boldsymbol{k},s} &= xe^{-iE_g t}c_{g\boldsymbol{k}s}(t) + ye^{-i(E_e+\omega_0)t}c_{e\boldsymbol{k}s}(t), \\ g_{\boldsymbol{k},s} &= -ye^{-i(E_g-\omega_0)t}c_{g\boldsymbol{k}s}(t) + xe^{-iE_e t}c_{e\boldsymbol{k}s}(t). \end{aligned} \tag{33}$$

In Eq. (33), we have set $x = \sqrt{\frac{\Omega+\omega_0}{2\Omega}}$ and $y = \sqrt{\frac{\Omega-\omega_0}{2\Omega}}$.

C. Spin polarization vector

Up to now, we have obtained the reduced density matrix of electrons; so the spin polarization vector $\boldsymbol{P} = \langle\boldsymbol{\sigma}\rangle = [\langle\sigma_x\rangle, \langle\sigma_y\rangle, \langle\sigma_z\rangle]$ can be calculated next. For any spatial direction $\boldsymbol{n} = (\sin\Theta\cos\Phi, \sin\Theta\sin\Phi, \cos\Theta)$, the projection average value of the operator $\boldsymbol{\sigma}$ on it is given by

$$\langle\boldsymbol{\sigma}\cdot\boldsymbol{n}\rangle = \mathrm{tr}(\rho_e\boldsymbol{\sigma}\cdot\boldsymbol{n}). \tag{34}$$

After performing the calculation, we have

$$\begin{aligned}\langle\boldsymbol{\sigma}\cdot\boldsymbol{n}\rangle &= 2\cos\Theta(p_1P_\uparrow^+ + p_2P_\uparrow^-) - \cos\Theta \\ &\quad + 2\sin\Theta\sum_{n=1}^{2} p_n \mathrm{Re}\left[e^{-i\Phi}\left(f_0^* g_0 + \sum_{\boldsymbol{k},s} f_{\boldsymbol{k},s}^* g_{\boldsymbol{k},s}\right)\right].\end{aligned} \tag{35}$$

Here, $P_\uparrow^\pm$ represents the probability that the electron's spin is up when it is in state $|\psi_\pm(t)\rangle$. Its expression reads as

$$\begin{aligned} P_\uparrow^\pm =& \left|xe^{-iE_g t}c_g(t) + ye^{-i(E_e+\omega_0)t}c_e(t)\right|^2 \\ &+ \sum_{\boldsymbol{k},s}[2xy\,\mathrm{Re}\{e^{-i(E_e-E_g+\omega_0)t}c_{g\boldsymbol{k}s}^* c_{e\boldsymbol{k}s}\} \\ &+ x^2|c_{g\boldsymbol{k}s}|^2 + y^2|c_{e\boldsymbol{k}s}|^2]. \end{aligned} \tag{36}$$

In addition,

$$\begin{aligned}\sum_{\boldsymbol{k},s} f_{\boldsymbol{k},s}^* g_{\boldsymbol{k},s} =& xye^{i\omega_0 t}\left(\sum_{\boldsymbol{k},s}|c_{e\boldsymbol{k}s}|^2 - \sum_{\boldsymbol{k},s}|c_{g\boldsymbol{k}s}|^2\right) \\ &- y^2 e^{i(E_e-E_g+2\omega_0)t}\sum_{\boldsymbol{k},s} c_{g\boldsymbol{k}s}c_{e\boldsymbol{k}s}^* \\ &+ x^2 e^{i(E_g-E_e)t}\sum_{\boldsymbol{k},s} c_{g\boldsymbol{k}s}^* c_{e\boldsymbol{k}s}.\end{aligned} \tag{37}$$

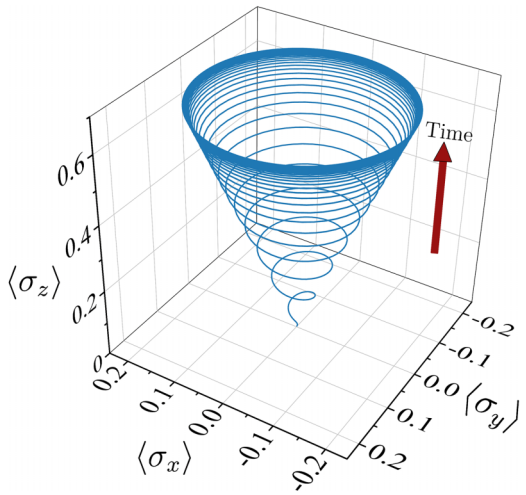

FIG. 1. The spatial trajectory of $\boldsymbol{P}$ with $\omega_0 = 0.05$ a.u. and $B_0 = 0.01$ a.u. The red arrow in the figure indicates the upward evolution of the helical curve over time.

It can be found that no matter whether we are solving (36) or (37), the calculation of the three terms $\sum_{\boldsymbol{k},s}|c_{e\boldsymbol{k}s}|^2$, $\sum_{\boldsymbol{k},s}|c_{g\boldsymbol{k}s}|^2$, and $\sum_{\boldsymbol{k},s} c_{g\boldsymbol{k}s}c_{e\boldsymbol{k}s}^*$ must be performed. Fortunately, we can apply the Weisskopf-Wigner approximation again to obtain (see Appendix B for details)

$$\begin{aligned}\sum_{\boldsymbol{k},s}|c_{g\boldsymbol{k}s}|^2 &= \frac{1}{4c^5}\int_0^t \mathscr{A}_1|c_e(t_1)|^2 + \mathscr{A}_2|c_g(t_1)|^2\mathrm{d}t_1, \\ \sum_{\boldsymbol{k},s}|c_{e\boldsymbol{k}s}|^2 &= \frac{1}{4c^5}\int_0^t \mathscr{A}_2|c_e(t_1)|^2\mathrm{d}t_1, \\ \sum_{\boldsymbol{k},s} c_{g\boldsymbol{k}s}^* c_{e\boldsymbol{k}s} &= -\frac{1}{4c^5}\int_0^t \mathscr{A}_2 c_g^*(t_1)c_e(t_1)\mathrm{d}t_1,\end{aligned} \tag{38}$$

where

$$\mathscr{A}_1 = \frac{8\Omega B_0^2}{3} + \frac{2B_0^4}{3\Omega}, \quad \mathscr{A}_2 = \frac{4\pi B_0^2}{3\Omega^2}\omega_0^3. \tag{39}$$

III. NUMERICAL RESULTS

In this paper, we are primarily concerned with the case where the electron is initially in a spin-unpolarized state. Therefore $\boldsymbol{P}_0 = 0$ and

$$\rho_S(0) = \tfrac{1}{2}(|\uparrow\rangle\langle\uparrow| + |\downarrow\rangle\langle\downarrow|) \otimes |0\rangle\langle 0|. \tag{40}$$

With the initial condition given by Eq. (40), we perform numerical calculations for the spin polarization vector $\boldsymbol{P}$. In Fig. 1, we present the spatial trajectory of $\boldsymbol{P}$ when $\omega_0 = 0.05$ a.u. and $B_0 = 0.01$ a.u. It can be found that under the action of a circularly polarized magnetic field, the spin polarization vector of electrons will spirally grow along the z-axis direction. Figure 2(a) quantitatively depicts the variation of $\langle\sigma_z\rangle$ with time, revealing that $\langle\sigma_z\rangle$ eventually reaches an upper limit of about 0.67. Additionally, we also show the functional relationship between $\langle\sigma_x\rangle$ and $\langle\sigma_y\rangle$ during the same time period in Fig. 2(b). The results reflect that the point $(\langle\sigma_x\rangle, \langle\sigma_y\rangle)$ ultimately lies on a fixed circle. This implies that $\boldsymbol{P}$ will reach a state of radiative equilibrium after a certain period of time

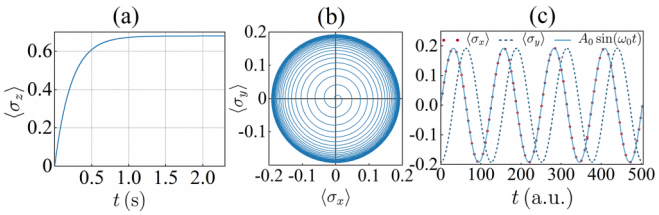

FIG. 2. The parameters ω_0 and B_0 are consistent with those in Fig. 1. (a) $\langle\sigma_z\rangle$ as a function of time. (b) The projection of $\boldsymbol{P}$ in the xy plane. (c) The time variation curves of $\langle\sigma_x\rangle$ and $\langle\sigma_y\rangle$. Here, $A_0 = 0.1924$, and $t = 0$ denotes a moment selected after the stabilization of $\langle\sigma_z\rangle$, at which $\langle\sigma_x\rangle = 0$.

and precess around the z axis. To further demonstrate this fact, we capture a segment of the curve depicting the variation of $\langle\sigma_x\rangle$ and $\langle\sigma_y\rangle$ with time after $\langle\sigma_z\rangle$ stabilized, as shown in Fig. 2(c). It is evident that both $\langle\sigma_x\rangle$ and $\langle\sigma_y\rangle$ exhibit simple harmonic vibration with the same amplitude and frequency over time, which is consistent with the description in Fig. 2(b). Also, it is crucial to note that the time curve corresponding to $\langle\sigma_y\rangle$ coincides perfectly with a sine function of frequency ω_0 and amplitude A_0. This shows that the precession frequency is exactly the frequency ω_0 of the circularly polarized magnetic field. Here, it should be emphasized that the dynamic properties of $\boldsymbol{P}$ mentioned above are acquired through numerical analysis rather than analytical expressions. This is because Eq. (35) cannot be simplified into a clear and straightforward expression. However, these dynamical properties are still applicable to other numerical examples (involving different values of ω_0 and B_0) that we discuss later, which is easy to check numerically.

Having understood the general dynamic properties of the polarization vector, it is natural to explore how the tunable parameters of the system affect its evolution. As shown in Fig. 3(a), we first calculate the maximum value (denoted by $\langle\sigma_z\rangle_{\max}$) that $\langle\sigma_z\rangle$ can reach for different B_0 and ω_0. Here, the maximum B_0 considered is only up to 10^{-2} a.u. ($\sim$2350 T) in order not to be far from reality. What is particularly

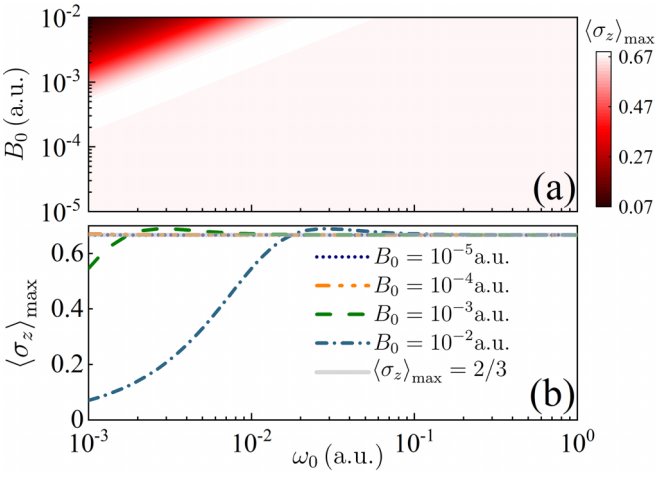

FIG. 3. (a) The maximum value of $\langle\sigma_z\rangle$ over time as a function of ω_0 and B_0. (b) Profile lines of the contour map in (a) for a given B_0.

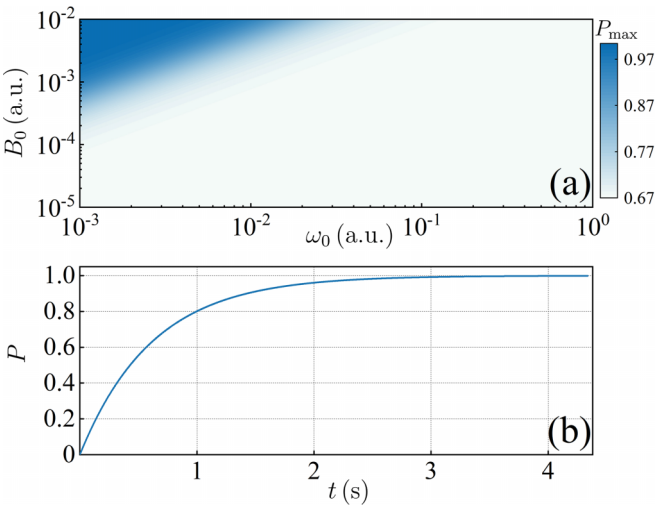

FIG. 4. (a) The maximum value of polarizability over time as a function of ω_0 and B_0. (b) Time-varying curve of P with $B_0 = 0.01$ a.u. and $\omega_0 = 0.001$ a.u.

intriguing is that there seems to be a significant area of parameter values where $\langle\sigma_z\rangle_{\max}$ is approximately 2/3. Moreover, within this area, there also appears to be a common characteristic: $\omega_0/B_0 \gg 1$. To confirm these two judgments, we present in Fig. 3(b) the curves depicting the variation of $\langle\sigma_z\rangle_{\max}$ with ω_0 for a given B_0, and the reference line $\langle\sigma_z\rangle_{\max} = 2/3$. It is clearly visible from the graph that as ω_0/B_0 gradually increases, the curves corresponding to different magnetic field intensities all converge to 2/3. This phenomenon is particularly evident for the curve with $B_0 = 0.01$ a.u.

Next, we also investigate the impact of ω_0 and B_0 on the maximum polarizability $P_{\max}$, and the results are shown in Fig. 4(a). It can be observed that similar to the behavior of $\langle\sigma_z\rangle_{\max}$, when $\omega_0/B_0 \gg 1$, $P_{\max}$ is about 0.67 and is independent of the specific values of ω_0 and B_0. This phenomenon bears a striking resemblance to the process in which the moving electrons in a storage ring are polarized due to the Sokolov-Ternov effect [41] under the action of a uniform magnetic field. The maximum polarizability of the latter is a fixed value as $8\sqrt{3}/15$ [41], with the magnetic field intensity and other system parameters only affecting the speed of polarization. Furthermore, it is exciting that the maximum polarizability corresponding to the parameter region in the upper left corner of Fig. 4(a) can be very close to 1. At the same time, as demonstrated in Fig. 4(b), by selecting $B_0 = 0.01$ a.u. and $\omega_0 = 0.001$ a.u., it only takes about about 5 s for electrons to be fully polarized.

IV. SUMMARY AND DISCUSSION

In summary, we rigorously address the time-dependent evolution of the spin polarization vector of electrons in a circularly polarized magnetic field. We find that electrons that are completely spin polarized can be attained by adjusting the intensity and frequency of the external magnetic field. Additionally, the polarization time can also be controlled on the order of seconds, which is highly significant for practical

applications, although a magnetic field intensity as high as 2×10^3 T is required here.

The theoretical model presented in this paper does not involve the spatial motion of electrons but only includes magnetic dipole interactions. Consequently, the corresponding speed of polarization is naturally inferior to that of the previously proposed schemes [29,31,41]. However, it should be noted that the probability of spin flip of electrons in these schemes during the radiation process is calculated based on perturbation theory. Obviously, the high degree of polarization implies that the transition probability is not a small quantity. This raises the question, Can perturbation theory and a high degree of polarization coexist self-consistently? Last but not least, the model presented in this paper can be regarded as a toy model that neglects spatial motion, allowing us to analytically (nonperturbatively) solve Eq. (10) due to its simplicity. Therefore it is worth exploring whether the polarizability can also be obtained nonperturbatively after considering the spatial motion of electrons.

ACKNOWLEDGMENT

This work was supported by the National Natural Science Foundation of China (Grants No. 12088101 and No. U2330401).

APPENDIX A

First, let us denote the polar angle and azimuthal angle of vector $\boldsymbol{k}$ as β and α, respectively. Then, the polarization vector $\boldsymbol{\epsilon}_{\boldsymbol{k},s}$ can be expressed by them as

$$\begin{aligned}\boldsymbol{\epsilon}_{\boldsymbol{k},1} &= (-\cos\beta\cos\alpha, -\cos\beta\sin\alpha, \sin\beta),\\ \boldsymbol{\epsilon}_{\boldsymbol{k},2} &= (-\sin\alpha, \cos\alpha, 0).\end{aligned} \tag{A1}$$

By comparing with θ_s and ϕ_s, we obtain

$$\begin{aligned}(-\cos\beta\cos\alpha, -\cos\beta\sin\alpha, \sin\beta) &= (\sin\theta_1\cos\phi_1, \sin\theta_1\sin\phi_1, \cos\theta_1),\\ (-\sin\alpha, \cos\alpha, 0) &= (\sin\theta_2\cos\phi_2, \sin\theta_2\sin\phi_2, \cos\theta_2).\end{aligned} \tag{A2}$$

Therefore, when $s = 1$, Eq. (12) can be transformed into

$$\begin{aligned}\langle g|\boldsymbol{\sigma}\cdot\boldsymbol{\epsilon}_{\boldsymbol{k},s}|g\rangle &= \frac{\omega_0}{\Omega}\sin\beta + \frac{\sqrt{2}B_0}{\Omega}\cos\beta\cos(\omega_0 t-\alpha),\\ \langle e|\boldsymbol{\sigma}\cdot\boldsymbol{\epsilon}_{\boldsymbol{k},s}|e\rangle &= -\frac{\omega_0}{\Omega}\sin\beta - \frac{\sqrt{2}B_0}{\Omega}\cos\beta\cos(\omega_0 t-\alpha),\\ \langle e|\boldsymbol{\sigma}\cdot\boldsymbol{\epsilon}_{\boldsymbol{k},s}|g\rangle &= e^{i\Omega t}\left[\frac{\sqrt{2}B_0}{\Omega}\sin\beta - \frac{\omega_0}{\Omega}\cos\beta\cos(\omega_0 t-\alpha) + i\cos\beta\sin(\omega_0 t-\alpha)\right].\end{aligned} \tag{A3}$$

With the help of Eq. (A3), we have

$$\begin{aligned}\int_0^{2\pi}\int_0^{\pi} f_{11}\sin\beta\,\mathrm{d}\beta\mathrm{d}\alpha =& \frac{8\pi\omega_0^2}{3\Omega^2} + \frac{4\pi B_0^2}{3\Omega^2}\cos[\omega_0(t-t_1)] + e^{i\Omega(t-t_1)}\left(\frac{2\pi\omega_0^2}{3\Omega^2}\cos[\omega_0(t-t_1)]\right.\\ &\left. + \frac{2\pi}{3}\cos[\omega_0(t-t_1)] - \frac{4i\pi\omega_0}{3\Omega}\sin[\omega_0(t-t_1)] + \frac{16\pi B_0^2}{3\Omega^2}\right),\end{aligned} \tag{A4}$$

$$\int_0^{2\pi}\int_0^{\pi} f_{22}\sin\beta\,\mathrm{d}\beta\mathrm{d}\alpha = \left(\int_0^{2\pi}\int_0^{\pi} f_{11}\sin\beta\,\mathrm{d}\beta\mathrm{d}\alpha\right)^*, \tag{A5}$$

$$\begin{aligned}\int_0^{2\pi}\int_0^{\pi} f_{12}\sin\beta\,\mathrm{d}\beta\mathrm{d}\alpha =& e^{i\Omega t_1}\left(\frac{2\sqrt{2}\pi B_0\omega_0}{3\Omega^2}\cos[\omega_0(t-t_1)] + \frac{2\sqrt{2}i\pi B_0}{3\Omega}\sin[\omega_0(t-t_1)] - \frac{8\sqrt{2}\pi B_0\omega_0}{3\Omega^2}\right)\\ &+ e^{i\Omega t}\left(\frac{8\sqrt{2}\pi B_0\omega_0}{3\Omega^2} - \frac{2\sqrt{2}\pi B_0\omega_0}{3\Omega^2}\cos\left[\omega_0(t-t_1)\right] + \frac{2\sqrt{2}i\pi B_0}{3\Omega}\sin[\omega_0(t-t_1)]\right),\end{aligned} \tag{A6}$$

$$\int_0^{2\pi}\int_0^{\pi} f_{21}\sin\beta\,\mathrm{d}\beta\mathrm{d}\alpha = \left(\int_0^{2\pi}\int_0^{\pi} f_{12}\sin\beta\,\mathrm{d}\beta\mathrm{d}\alpha\right)^* (t \longleftrightarrow t_1). \tag{A7}$$

Here, we omit a common factor $\frac{\pi\omega}{2c^2}e^{-i\omega_k(t-t_1)}$ in Eqs. (A4)–(A7) for convenience.

Similarly, when $s = 2$, the corresponding calculations are accessible. Finally, by combining the contributions of $s = 1$ and $s = 2$, the expression of matrix element F_{ij} is given by

$$F_{11} = \frac{8\pi\omega_0^2}{3\Omega^2} + \frac{16\pi B_0^2}{3\Omega^2}\cos[\omega_0(t-t_1)] + e^{i\Omega(t-t_1)}\left(\frac{16\pi B_0^2}{3\Omega^2} + \frac{8\pi\omega_0^2}{3\Omega^2}\cos[\omega_0(t-t_1)]\right.$$
$$\left. + \frac{8\pi}{3}\cos[\omega_0(t-t_1)] - \frac{16i\pi\omega_0}{3\Omega}\sin[\omega_0(t-t_1)]\right), \tag{A8}$$

$$F_{22} = \frac{8\pi\omega_0^2}{3\Omega^2} + \frac{16\pi B_0^2}{3\Omega^2}\cos[\omega_0(t-t_1)] + e^{-i\Omega(t-t_1)}\left(\frac{16\pi B_0^2}{3\Omega^2} + \frac{8\pi\omega_0^2}{3\Omega^2}\cos[\omega_0(t-t_1)]\right.$$
$$\left. + \frac{8\pi}{3}\cos[\omega_0(t-t_1)] + \frac{16i\pi\omega_0}{3\Omega}\sin[\omega_0(t-t_1)]\right), \tag{A9}$$

$$F_{12} = e^{i\Omega t_1}\left(-\frac{8\sqrt{2}\pi B_0\omega_0}{3\Omega^2} + \frac{8\sqrt{2}\pi B_0\omega_0}{3\Omega^2}\cos[\omega_0(t-t_1)] + \frac{8\sqrt{2}i\pi B_0}{3\Omega}\sin[\omega_0(t-t_1)]\right)$$
$$+ e^{i\Omega t}\left(\frac{8\sqrt{2}\pi B_0\omega_0}{3\Omega^2} - \frac{8\sqrt{2}\pi B_0\omega_0}{3\Omega^2}\cos[\omega_0(t-t_1)] + \frac{8\sqrt{2}i\pi B_0}{3\Omega}\sin[\omega_0(t-t_1)]\right), \tag{A10}$$

$$F_{21} = e^{-i\Omega t}\left(-\frac{8\sqrt{2}\pi B_0\omega_0}{3\Omega^2} + \frac{8\sqrt{2}\pi B_0\omega_0}{3\Omega^2}\cos[\omega_0(t-t_1)] + \frac{8\sqrt{2}i\pi B_0}{3\Omega}\sin[\omega_0(t-t_1)]\right)$$
$$+ e^{-i\Omega t_1}\left(\frac{8\sqrt{2}\pi B_0\omega_0}{3\Omega^2} - \frac{8\sqrt{2}\pi B_0\omega_0}{3\Omega^2}\cos[\omega_0(t-t_1)] + \frac{8\sqrt{2}i\pi B_0}{3\Omega}\sin[\omega_0(t-t_1)]\right). \tag{A11}$$

APPENDIX B

According to Eq. (10), we have

$$\sum_{\boldsymbol{k},s}|c_{g\boldsymbol{k}s}|^2 = \frac{1}{(2\pi)^3}\sum_s\int\left|\int_0^t u_1(t_1)c_e^*(t_1) + u_2(t_1)c_g^*(t_1)\mathrm{d}t_1\right|^2\mathrm{d}\boldsymbol{k}$$
$$= \frac{1}{(2\pi)^3}\int_0^t\int_0^t\int_0^\infty\int_0^{2\pi}\int_0^\pi\sum_s[u_1(t_1)u_1^*(t_2)c_e^*(t_1)c_e(t_2) + u_2(t_1)u_2^*(t_2)c_g^*(t_1)c_g(t_2)$$
$$+ u_1(t_1)u_2^*(t_2)c_e^*(t_1)c_g(t_2) + u_2(t_1)u_1^*(t_2)c_g^*(t_1)c_e(t_2)]\omega^2\sin\beta\,\mathrm{d}\beta\mathrm{d}\alpha\mathrm{d}\omega\mathrm{d}t_1\mathrm{d}t_2, \tag{B1}$$

$$\sum_{\boldsymbol{k},s}|c_{e\boldsymbol{k}s}|^2 = \frac{1}{(2\pi)^3}\sum_s\int\left|\int_0^t w_1(t_1)c_e^*(t_1) + w_2(t_1)c_g^*(t_1)\mathrm{d}t_1\right|^2\mathrm{d}\boldsymbol{k}$$
$$= \frac{1}{(2\pi)^3}\int_0^t\int_0^t\int_0^\infty\int_0^{2\pi}\int_0^\pi\sum_s[w_1(t_1)w_1^*(t_2)c_e^*(t_1)c_e(t_2) + w_2(t_1)w_2^*(t_2)c_g^*(t_1)c_g(t_2)$$
$$+ w_1(t_1)w_2^*(t_2)c_e^*(t_1)c_g(t_2) + w_2(t_1)w_1^*(t_2)c_g^*(t_1)c_e(t_2)]\omega^2\sin\beta\,\mathrm{d}\beta\mathrm{d}\alpha\mathrm{d}\omega\mathrm{d}t_1\mathrm{d}t_2, \tag{B2}$$

and

$$\sum_{\boldsymbol{k},s}c_{g\boldsymbol{k}s}^*c_{e\boldsymbol{k}s} = \frac{1}{(2\pi)^3}\int_0^t\int_0^t\int_0^\infty\int_0^{2\pi}\int_0^\pi\sum_s[u_1(t_1)w_1^*(t_2)c_e^*(t_1)c_e(t_2) + u_2(t_1)w_1^*(t_2)c_g^*(t_1)c_e(t_2)$$
$$+ u_1(t_1)w_2^*(t_2)c_e^*(t_1)c_g(t_2) + u_2(t_1)w_2^*(t_2)c_g^*(t_1)c_g(t_2)]\omega^2\sin\beta\,\mathrm{d}\beta\mathrm{d}\alpha\mathrm{d}\omega\mathrm{d}t_1\mathrm{d}t_2. \tag{B3}$$

It is evident that the integration of β and α in Eqs. (B1)–(B3) can be readily replicated following the procedures outlined in Appendix A. Having done so, Eq. (38) can naturally be obtained by again using the Weisskopf-Wigner approximation.

[1] C. Prescott, W. Atwood, R. Cottrell, H. DeStaebler, E. L. Garwin, A. Gonidec, R. H. Miller, L. S. Rochester, T. Sato, D. J. Sherden, C. K. Sinclair, S. Stein, R. E. Taylor, J. E. Clendenin, V. W. Hughes, N. Sasao, K. P. Schüler, M. G. Borghini, K. Lübelsmeyer, and W. Jentschke, Parity non-conservation in inelastic electron scattering, Phys. Lett. B **77**, 347 (1978).

[2] Y. S. Tsai, Production of polarized τ pairs and tests of CP violation using polarized $e^{\pm}$ colliders near threshold, Phys. Rev. D **51**, 3172 (1995).

[3] J. Erler, C. J. Horowitz, S. Mantry, and P. A. Souder, Weak polarized electron scattering, Annu. Rev. Nucl. Part. Sci. **64**, 269 (2014).

[4] W. Armstrong, H. Kang, A. Liyanage, J. Maxwell, J. Mulholland, L. Ndukum, A. Ahmidouch, I. Albayrak, A. Asaturyan, O. Ates, H. Baghdasaryan, W. Boeglin, P. Bosted, E. Brash, C. Butuceanu, M. Bychkov, P. Carter, C. Chen, J.-P. Chen, S. Choi *et al.* (SANE Collaboration), Revealing color forces with transverse polarized electron scattering, Phys. Rev. Lett. **122**, 022002 (2019).

[5] T. Donnelly and A. Raskin, Considerations of polarization in inclusive electron scattering from nuclei, Ann. Phys. (Amsterdam) **169**, 247 (1986).

[6] P. L. Anthony, R. G. Arnold, C. Arroyo, K. Baird, K. Bega, J. Biesiada, P. E. Bosted, M. Breuer, R. Carr, G. D. Cates, J.-P. Chen, E. Chudakov, M. Cooke, F. J. Decker, P. Decowski, A. Deur, W. Emam, R. Erickson, T. Fieguth, C. Field *et al.* (SLAC E158 Collaboration), Observation of parity nonconservation in Møller scattering, Phys. Rev. Lett. **92**, 181602 (2004).

[7] C. A. Aidala, S. D. Bass, D. Hasch, and G. K. Mallot, The spin structure of the nucleon, Rev. Mod. Phys. **85**, 655 (2013).

[8] U. Kolac, M. Donath, K. Ertl, H. Liebl, and V. Dose, High-performance GaAs polarized electron source for use in inverse photoemission spectroscopy, Rev. Sci. Instrum. **59**, 1933 (1988).

[9] F. Ciccacci, S. De Rossi, E. Pelucchi, and A. Tagliaferri, Spin-resolved electron spectroscopy with highly polarized sources: Inverse photoemission from ferromagnets, Rev. Sci. Instrum. **68**, 1841 (1997).

[10] J. Berakdar, Probing the spin polarization in ferromagnets, Phys. Rev. Lett. **83**, 5150 (1999).

[11] S. N. Samarin, J. Berakdar, O. Artamonov, and J. Kirschner, Visualizing spin-dependent electronic collisions in ferromagnets, Phys. Rev. Lett. **85**, 1746 (2000).

[12] F. O. Schumann, C. Winkler, J. Kirschner, F. Giebels, H. Gollisch, and R. Feder, Spin-resolved mapping of spin contribution to exchange-correlation holes, Phys. Rev. Lett. **104**, 087602 (2010).

[13] P. S. Farago, Electron optic dichroism and electron optic activity, J. Phys. B **14**, L743 (1981).

[14] T. Gay, Physics and technology of polarized electron scattering from atoms and molecules, Adv. At. Mol. Opt. Phys. **57**, 157 (2009).

[15] D. T. Pierce and F. Meier, Photoemission of spin-polarized electrons from GaAs, Phys. Rev. B **13**, 5484 (1976).

[16] M. Alguard, J. Clendenin, R. Ehrlich, V. Hughes, J. Ladish, M. Lubell, K. Schüler, G. Baum, W. Raith, R. Miller, and W. Lysenko, A source of highly polarized electrons at the Stanford linear accelerator center, Nucl. Instrum. Methods **163**, 29 (1979).

[17] W. von Drachenfels, U. Koch, T. Müller, W. Paul, and H. Schaefer, A pulsed source for polarized electrons with high repetition rate, Nucl. Instrum. Methods **140**, 47 (1977).

[18] P. F. Wainwright, M. J. Alguard, G. Baum, and M. S. Lubell, Application of a dc Fano effect polarized electron source to low-energy electron–atom scattering, Rev. Sci. Instrum. **49**, 571 (1978).

[19] E. Kisker, G. Baum, A. H. Mahan, W. Raith, and B. Reihl, Electron field emission from ferromagnetic europium sulfide on tungsten, Phys. Rev. B **18**, 2256 (1978).

[20] E. Garwin, F. Meier, D. Pierce, K. Sattler, and H.-C. Siegmann, A pulsed source of spin-polarized electrons by photoemission from EuO, Nucl. Instrum. Methods **120**, 483 (1974).

[21] L. G. Gray, K. W. Giberson, C. Cheng, R. S. Keiffer, F. B. Dunning, and G. K. Walters, Intense source of spin-polarized electrons using laser-induced optical pumping, Rev. Sci. Instrum. **54**, 271 (1983).

[22] D. T. Pierce, R. J. Celotta, G. Wang, W. N. Unertl, A. Galejs, C. E. Kuyatt, and S. R. Mielczarek, The GaAs spin polarized electron source, Rev. Sci. Instrum. **51**, 478 (1980).

[23] T. Maruyama, E. L. Garwin, R. Prepost, and G. H. Zapalac, Electron-spin polarization in photoemission from strained GaAs grown on $GaAs_{1-x}P_x$, Phys. Rev. B **46**, 4261 (1992).

[24] Y. Kurihara, T. Omori, Y. Takeuchi, M. Yoshioka, T. Nakanishi, S. Okumi, M. Tawada, K. Togawa, M. Tsubata, T. Baba, M. Mizuta, R. K. Alley, H. Aoyagi, J. E. Clendenin, J. C. Frisch, G. A. Mulhollan, P. J. Sáez, D. C. Schultz, H. Tang, and K. H. Witte, A high polarization and high quantum efficiency photocathode using a GaAs–AlGaAs superlattice, Jpn. J. Appl. Phys. **34**, 355 (1995).

[25] H. M. Al-Khateeb, B. G. Birdsey, T. C. Bowen, A. S. Green, M. E. Johnston, and T. J. Gay, A simplified GaAs polarized electron source, Rev. Sci. Instrum. **70**, 3882 (1999).

[26] G. Mourou, Nobel lecture: Extreme light physics and application, Rev. Mod. Phys. **91**, 030501 (2019).

[27] J. W. Yoon, C. Jeon, J. Shin, S. K. Lee, H. W. Lee, I. W. Choi, H. T. Kim, J. H. Sung, and C. H. Nam, Achieving the laser intensity of 5.5×10^{22} W/cm^2 with a wavefront-corrected multi-PW laser, Opt. Express **27**, 20412 (2019).

[28] J. W. Yoon, Y. G. Kim, I. W. Choi, J. H. Sung, H. W. Lee, S. K. Lee, and C. H. Nam, Realization of laser intensity over 10^{23} W/cm^2, Optica **8**, 630 (2021).

[29] D. Del Sorbo, D. Seipt, T. G. Blackburn, A. G. R. Thomas, C. D. Murphy, J. G. Kirk, and C. P. Ridgers, Spin polarization of electrons by ultraintense lasers, Phys. Rev. A **96**, 043407 (2017).

[30] D. D. Sorbo, D. Seipt, A. G. R. Thomas, and C. P. Ridgers, Electron spin polarization in realistic trajectories around the magnetic node of two counter-propagating, circularly polarized, ultra-intense lasers, Plasma Phys. Controlled Fusion **60**, 064003 (2018).

[31] Y.-F. Li, R. Shaisultanov, K. Z. Hatsagortsyan, F. Wan, C. H. Keitel, and J.-X. Li, Ultrarelativistic electron-beam polarization in single-shot interaction with an ultraintense laser pulse, Phys. Rev. Lett. **122**, 154801 (2019).

[32] A. Gonoskov, T. G. Blackburn, M. Marklund, and S. S. Bulanov, Charged particle motion and radiation in strong electromagnetic fields, Rev. Mod. Phys. **94**, 045001 (2022).

[33] L. D. Landau, *The Classical Theory of Fields* (Elsevier, New York, 2013), Vol. 2.

[34] O. V. Kibis, Floquet theory of spin dynamics under circularly polarized light pulses, Phys. Rev. A **105**, 043106 (2022).

[35] R. J. Glauber, Coherent and incoherent states of the radiation field, Phys. Rev. **131**, 2766 (1963).

[36] R. Ekman and A. Ilderton, Backreaction in strong field QED: A toy model, Phys. Rev. D **101**, 056022 (2020).

[37] V. Weisskopf and E. Wigner, Berechnung der natürlichen Linienbreite auf Grund der Diracschen Lichttheorie, Z. Phys. **63**, 54 (1930).

[38] G. Grynberg, A. Aspect, C. Fabre, and C. Cohen-Tannoudji, *Introduction to Quantum Optics: From the Semi-classical Approach to Quantized Light* (Cambridge University Press, Cambridge, 2010).

[39] B. King and H. Hu, Classical and quantum dynamics of a charged scalar particle in a background of two counterpropagating plane waves, Phys. Rev. D **94**, 125010 (2016).

[40] J. G. Kirk, Radiative trapping in intense laser beams, Plasma Phys. Controlled Fusion **58**, 085005 (2016).

[41] S. R. Mane, Y. M. Shatunov, and K. Yokoya, Spin-polarized charged particle beams in high-energy accelerators, Rep. Prog. Phys. **68**, 1997 (2005).